pirical equation of state analogous to the ideal gas law (*30*)

$$P = Cn^{x}(k_{B}T)^{y} \quad (4)$$

where P is the pressure of the 2D gas, $x = 2/(1 + b) = 0.95(5)$, $y = 2b/(1 + b) = 1.05(5)$, $C = 0.8(2)(td^2)^w$ is a constant, and $w = (1 - b)/(1 + b) = -0.05(5)$.

Finally, we observe a weak dependence of the critical entropy per particle on the atomic interaction. Noting that a weakly interacting 2D Bose gas follows similar scaling laws near $\mu = 0$ (*18*) because it belongs to the same underlying dilute Bose gas universality class (*2*, *32*), we apply similar analysis and extract the critical entropy per particle S_c/N at four interaction strengths $g \approx 0.05$, 0.13, 0.19, 0.26, shown together with the lattice data ($g \approx 2.4$) in Fig. 4B. We observe a slow growing of S_c/N with g, and compare the measurements with mean-field calculations. The measured S_c/N is systematically lower than the mean-field predictions, potentially as a consequence of quantum critical physics. The weak dependence on the interaction strength can be captured by a power-law fit to the data as $S_c/Nk_B = 1.6(1)g^{0.18(2)}$.

In summary, on the basis of in situ density measurements of Bose gases in 2D optical lattices, we confirm the quantum criticality near the vacuum-to-superfluid quantum phase transition. Our experimental methods hold promise for identifying general quantum phase transitions, and prepare the tools for investigating quantum critical dynamics.

References and Notes

1. P. Coleman, A. J. Schofield, *Nature* **433**, 226 (2005).
2. S. Sachdev, *Quantum Phase Transitions* (Cambridge Univ. Press, Cambridge, 1999).
3. D. van der Marel *et al.*, *Nature* **425**, 271 (2003).
4. H. v. Löhneysen, A. Rosch, M. Vojta, P. Wölfle, *Rev. Mod. Phys.* **79**, 1015 (2007).
5. P. Gegenwart, Q. Si, F. Steglich, *Nat. Phys.* **4**, 186 (2008).
6. S. Sachdev, *Nat. Phys.* **4**, 173 (2008).
7. U. Al Khawaja, H. Stoof, *Nature* **411**, 918 (2001).
8. T. Senthil, A. Vishwanath, L. Balents, S. Sachdev, M. P. A. Fisher, *Science* **303**, 1490 (2004).
9. S. Sachdev, M. Müller, *J. Phys. Condens. Matter* **21**, 164216 (2009).
10. S. E. Sebastian *et al.*, *Nature* **441**, 617 (2006).
11. R. Coldea *et al.*, *Science* **327**, 177 (2010).
12. R. Jaramillo, Y. Feng, J. Wang, T. F. Rosenbaum, *Proc. Natl. Acad. Sci. U.S.A.* **107**, 13631 (2010).
13. M. Greiner, O. Mandel, T. Esslinger, T. W. Hänsch, I. Bloch, *Nature* **415**, 39 (2002).
14. K. Baumann, C. Guerlin, F. Brennecke, T. Esslinger, *Nature* **464**, 1301 (2010).
15. E. Haller *et al.*, *Nature* **466**, 597 (2010).
16. J. Simon *et al.*, *Nature* **472**, 307 (2011).
17. T. Donner *et al.*, *Science* **315**, 1556 (2007).
18. C.-L. Hung, X. Zhang, N. Gemelke, C. Chin, *Nature* **470**, 236 (2011).
19. R. Löw *et al.*, *Phys. Rev. A* **80**, 033422 (2009).
20. S. Trotzky *et al.*, *Nat. Phys.* **6**, 998 (2010).
21. Q. Zhou, T.-L. Ho, *Phys. Rev. Lett.* **105**, 245702 (2010).
22. K. R. A. Hazzard, E. J. Mueller, *Phys. Rev. A* **84**, 013604 (2011).
23. S. Fang, C.-M. Chung, P.-N. Ma, P. Chen, D.-W. Wang, *Phys. Rev. A* **83**, 031605(R) (2011).
24. Y. Kato, Q. Zhou, N. Kawashima, N. Trivedi, *Nat. Phys.* **4**, 617 (2008).
25. M. P. A. Fisher, P. B. Weichman, G. Grinstein, D. S. Fisher, *Phys. Rev. B* **40**, 546 (1989).
26. N. Gemelke, X. Zhang, C.-L. Hung, C. Chin, *Nature* **460**, 995 (2009).
27. C.-L. Hung, X. Zhang, N. Gemelke, C. Chin, *Phys. Rev. Lett.* **104**, 160403 (2010).
28. X. Zhang, C.-L. Hung, S.-K. Tung, N. Gemelke, C. Chin, *New J. Phys.* **13**, 045011 (2011).
29. B. Capogrosso-Sansone *et al.*, *New J. Phys.* **12**, 043010 (2010).
30. Materials and methods are available as supporting online material on *Science* Online.
31. T. Yefsah, R. Desbuquois, L. Chomaz, K. J. Günter, J. Dalibard, *Phys. Rev. Lett.* **107**, 130401 (2011).
32. S. Sachdev, E. R. Dunkel, *Phys. Rev. B* **73**, 085116 (2006).

Acknowledgments: We thank N. Prokof'ev and D.-W. Wang for discussions and numerical data; Q. Zhou, K. Hazzard, and N. Trivedi for discussions; and N. Gemelke and C. Parker for discussions and reading of the manuscript. The work was supported by NSF (grants PHY-0747907 and NSF-MRSEC DMR-0213745), the Packard foundation, and a grant from the Army Research Office with funding from the Defense Advanced Research Projects Agency Optical Lattice Emulator program. The data presented in this paper are available upon request sent to cchin@uchicago.edu.

Supporting Online Material

www.sciencemag.org/cgi/content/full/science.1217990/DC1
Materials and Methods
Fig. S1
References (*33*, *34*)

15 December 2011; accepted 30 January 2012
Published online 16 February 2012;
10.1126/science.1217990

Reactions of Solvated Electrons Initiated by Sodium Atom Ionization at the Vacuum-Liquid Interface

William A. Alexander,[1] Justin P. Wiens,[2] Timothy K. Minton,[1]* Gilbert M. Nathanson[2]*

Solvated electrons are powerful reagents in the liquid phase that break chemical bonds and thereby create additional reactive species, including hydrogen atoms. We explored the distinct chemistry that ensues when electrons are liberated near the liquid surface rather than within the bulk. Specifically, we detected the products resulting from exposure of liquid glycerol to a beam of sodium atoms. The Na atoms ionized in the surface region, generating electrons that reacted with deuterated glycerol, $C_3D_5(OD)_3$, to produce D atoms, D_2, D_2O, and glycerol fragments. Surprisingly, 43 ± 4% of the D atoms traversed the interfacial region and desorbed into vacuum before attacking C-D bonds to produce D_2.

Radiolysis experiments provide fundamental insights into electron reactivity in protic liquids such as water and alcohols through the use of ionizing reagents, including gamma rays and high-energy electrons, which penetrate deeply into solution. These reagents energize and ionize solvent molecules, creating hydrogen atoms and other free radicals, as well as solvated electrons, e_s^-, often in high enough concentrations to react with each other (*1*, *2*). Electrons and radicals created at the vacuum-liquid interface may behave differently from those in the bulk because of their partial solvation (*3*–*6*) and because transient neutral intermediates may evaporate before reacting further. Recent photoionization experiments show that partially to fully solvated electrons persist for $\geq 10^{-10}$ s at the surface of water, potentially leading to enhanced destruction of organic molecules in contact with these electrons (*6*–*8*). Molecular beam methods, using gas-phase sodium atoms as neutral precursors, provide a previously unexplored alternative for generating interfacial electrons in protic liquids. These electrons initiate a wide range of chemical events, including the production of atomic and molecular radicals that react at and near the surface or escape by evaporating from solution.

We performed the experiments by directing a weak effusive beam of sodium atoms at the surface of a liquid glycerol (1,2,3-propanetriol) film in vacuum. These Na atoms rapidly ionize into Na_s^+ and e_s^- in the interfacial region. We chose glycerol because of its low vapor pressure (10^{-4} torr) and water-like ability to solvate ions and electrons (*9*, *10*). Solvated electrons react in more diverse ways with alcohols than with water. In the latter case, the primary pathways are slow dissociation, $e_s^- + H_2O \rightarrow H + OH^-$, and fast recombination, $2e_s^- + 2H_2O \rightarrow H_2 + 2OH^-$ (*2*, *11*). The low flux of our effusive Na beam ensures that similar electron-electron recombination and additional radical-radical reactions do not compete with electron-solvent and radical-solvent reactions, whereas the soft landing and gentle ionization of Na generates elec-

[1]Department of Chemistry and Biochemistry, Montana State University, Bozeman, MT 59717, USA. [2]Department of Chemistry, University of Wisconsin, Madison, WI 53706, USA.

*To whom correspondence should be addressed. E-mail: tminton@montana.edu (T.K.M.); gmnathan@wisc.edu (G.M.N.)

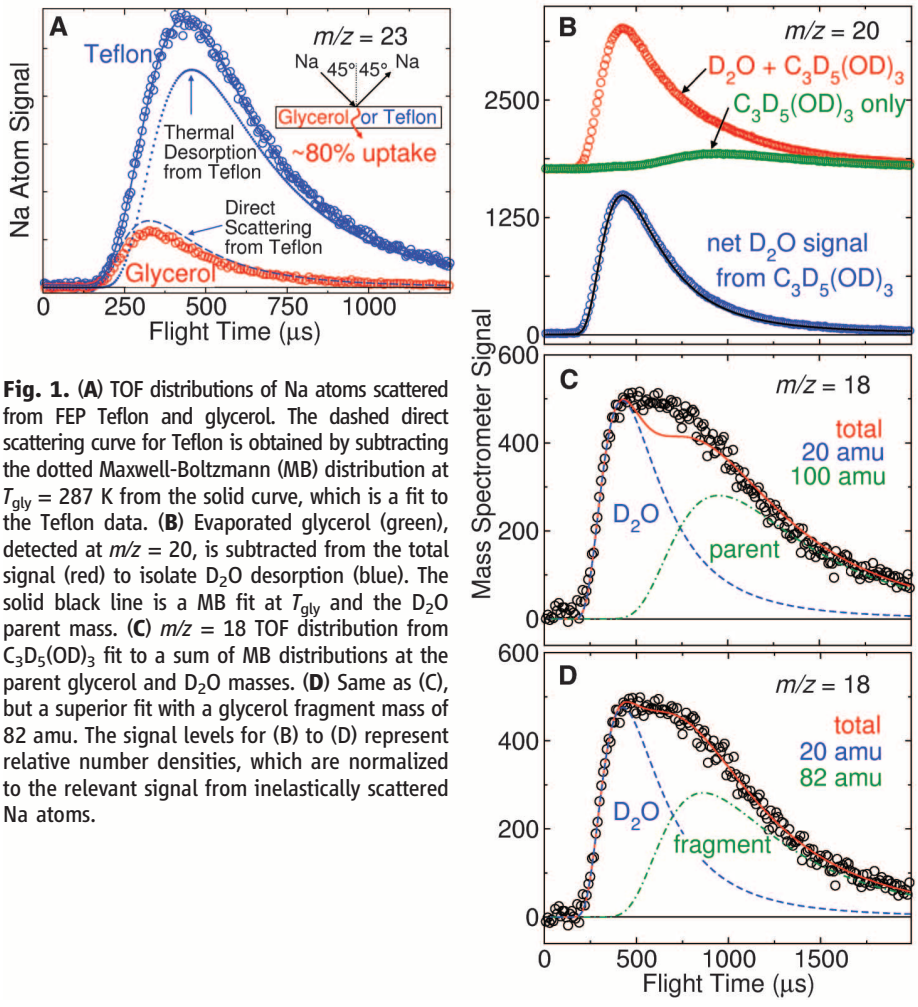

Fig. 1. (**A**) TOF distributions of Na atoms scattered from FEP Teflon and glycerol. The dashed direct scattering curve for Teflon is obtained by subtracting the dotted Maxwell-Boltzmann (MB) distribution at T_{gly} = 287 K from the solid curve, which is a fit to the Teflon data. (**B**) Evaporated glycerol (green), detected at m/z = 20, is subtracted from the total signal (red) to isolate D_2O desorption (blue). The solid black line is a MB fit at T_{gly} and the D_2O parent mass. (**C**) m/z = 18 TOF distribution from $C_3D_5(OD)_3$ fit to a sum of MB distributions at the parent glycerol and D_2O masses. (**D**) Same as (C), but a superior fit with a glycerol fragment mass of 82 amu. The signal levels for (B) to (D) represent relative number densities, which are normalized to the relevant signal from inelastically scattered Na atoms.

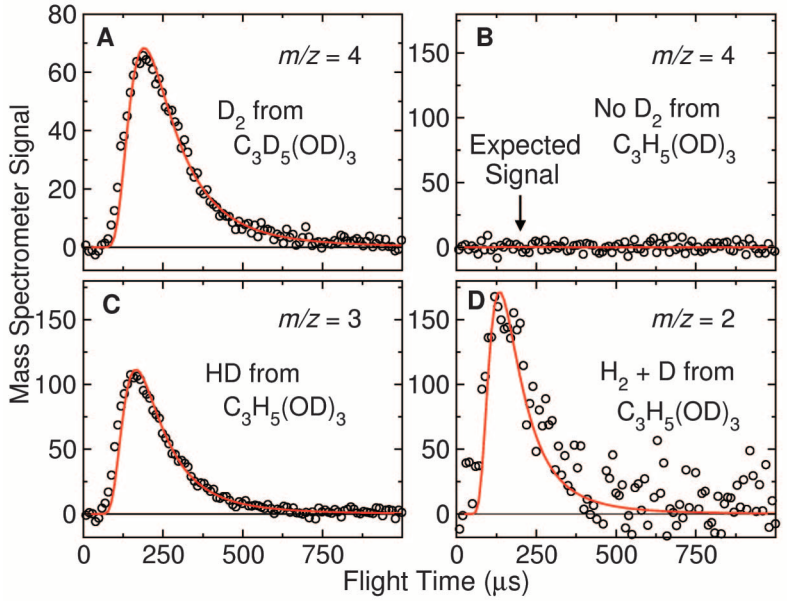

Fig. 2. TOF distributions of molecular hydrogen isotopologues: (**A**) D_2 from $C_3D_5(OD)_3$, (**B**) D_2 from $C_3H_5(OD)_3$, (**C**) HD from $C_3H_5(OD)_3$, and (**D**) H_2 + D from $C_3H_5(OD)_3$. The contribution from evaporated glycerol has been subtracted from each distribution. The solid red curves are MB fits at T_{gly} = 287 K.

trons in the absence of high-energy excitations. As shown below, reactions between these electrons and glycerol generate atomic and molecular hydrogen, water, and glycerol fragments within an estimated depth of 50 Å.

The continuously refreshed glycerol film, 0.1 mm thick, was held at 287 K during Na-atom exposure (fig. S1) (*12*, *13*). To delineate the reaction pathways, we used both $C_3H_5(OD)_3$ and $C_3D_5(OD)_3$ isotopologues. The velocity and angular distributions of the scattered Na atoms and desorbed reaction products were monitored by a rotatable mass spectrometer (*14*). Product signals were recorded as time-of-flight (TOF) distributions after the stream of molecules exiting the liquid surface was divided into pulses by a spinning slotted wheel. The Na oven (held at 670 K) produced a nearly effusive beam that deposited ~1 monolayer of Na atoms on the glycerol film during its 0.2-s exposure time.

Na-atom uptake into glycerol is explored in Fig. 1A, which compares the Na-atom signal after collision with the glycerol film to that obtained from FEP (fluorinated ethylene propylene) Teflon, presumed to be much less reactive than glycerol. The strength of the integrated flux from Teflon is ~4 times that from glycerol, implying that at least ~80% of the impinging Na atoms dissolve into glycerol and do not escape. The recorded distribution of Na atoms scattered from Teflon was decomposed into two components corresponding to (i) Na atoms that scatter directly (higher velocities and shorter arrival times; dashed line) and (ii) those that fully dissipate their energy at the surface and then thermally desorb in a Maxwell-Boltzmann (MB) distribution at the glycerol temperature of T_{gly} = 287 K (lower velocities and longer arrival times; dotted line). The glycerol distribution mimics direct scattering from Teflon and is entirely missing the thermal desorption component. Thus, Na atoms that thermally equilibrate on the glycerol film do not desorb into vacuum but instead remain in contact with glycerol molecules. The absence of thermally desorbed Na atoms implies that they ionize into Na_s^+ and e_s^- before motions of the surface glycerol molecules can propel the atoms back into the gas phase. Ab initio molecular dynamics simulations of Na-atom collisions with H_2O clusters corroborate this rapid interfacial ionization and show that surface water molecules reorient to point their OH groups toward the evolving Na_s^+ and e_s^- (*15*). The high density of OH groups in glycerol likely promotes both the immediate Na ionization inferred here and the subnanosecond solvation of electrons in the bulk (*10*). Reactions of these ionizing Na atoms with solvent glycerol may occur through direct electron transfer from Na to glycerol (*16*) or after partial or full electron solvation to form contact Na^+/e^- ion pairs or solvent-separated ions and electrons (*17*, *18*).

Analysis of the observed product signals revealed that electrons from Na atoms react with $C_3D_5(OD)_3$ to generate four volatile species: D

atoms, D_2, D_2O, and glycerol fragments. The D atoms are created close enough to the surface that nearly half of them escape into the vacuum before reacting with the solvent or with each other.

We observed copious water production from both glycerol isotopologues upon Na-atom exposure. Figure 1B shows D_2O desorption from $C_3D_5(OD)_3$ detected at a mass-to-charge ratio m/z = 20 (D_2O^+). This desorption is accompanied by the natural evaporation of intact glycerol molecules, which appear at m/z = 20 through dissociative ionization in the mass spectrometer. The D_2O product molecules desorb with a MB velocity distribution at T_{gly} (blue curve fit to the net D_2O signal) and a cosine angular distribution (fig. S2). These good fits demonstrate that reactions of e_s^- create D_2O molecules that thermally equilibrate before desorbing into vacuum. D_2O may be produced by ionic and neutral routes, as established in previous radiolysis studies of bulk liquid ethanol (*19*) and ethylene glycol (*20*). In the ionic pathway, an electron attacks solvent glycerol to make hydroxide, $e_s^- + C_3D_5(OD)_3 \rightarrow {\bullet}C_3D_5(OD)_2 + OD^-$, followed by an acid-base reaction, $C_3D_5(OD)_3 + OD^- \rightarrow D_2O + C_3D_5(OD)_2O^-$ (*19*). A second, neutral pathway involves D-atom attack on solvent glycerol to make D_2 and ${\bullet}C_3D_4(OD)_3$, which subsequently decomposes into D_2O and the open-shell ketone ${\bullet}CD_2COCD_2OD$ (*20*).

Figure 1, C and D, provides evidence for one or both D_2O channels through identification of the matching glycerol fragments. The TOF distribution, monitored at m/z = 18 (OD^+), is much broader than expected for pure D_2O desorption even after subtracting the parent glycerol signal. Figure 1C shows an attempt to fit this long–arrival time component with evaporation of parent glycerol (100 amu): The poor fit indicates that this component cannot be explained by glycerol desorption created by Na-atom sputtering or the local heat of reaction. Instead, the extra signal in Fig. 1D can be well fit by a MB distribution in the mass range of 78 to 84 amu. This range is consistent with evaporation of the ${\bullet}C_3D_5(OD)_2$ and ${\bullet}CD_2COCD_2OD$ radicals and their closed-shell products after abstracting a D atom from a neighboring glycerol molecule (*13*). To the extent that it occurs, the desorption of the radical species provides a means to halt their decomposition and the associated chain reactions that occur in the bulk (*20*).

Na ionization also initiates reactions that generate molecular hydrogen, as shown in Fig. 2. As with D_2O, the D_2 molecules arising from reactions with $C_3D_5(OD)_3$ in Fig. 2A are fit well by MB velocity (solid lines) and cosine angular distributions (fig. S2). This D_2 production implies that D atoms are created by electron-induced dissociation of O-D and C-D bonds, after which the D atom abstracts a second D atom from the solvent. We found that D_2 is not produced from the mixed isotopologue, $C_3H_5(OD)_3$, as shown in Fig. 2B. The absence of D_2 in this case has two implications. First, D atoms created by e_s^- near the surface are not energetic enough to overcome the high activation energy for D-atom abstraction from O-D bonds (*21*). In the case of $C_3D_5(OD)_3$ in Fig. 2A, D_2 must instead arise from D-atom abstraction from a C-D bond. Second, D atoms react with solvent glycerol faster than they can react with each other ($D + D \rightarrow D_2$) at our low Na beam flux. The missing D_2 signal from $C_3H_5(OD)_3$ instead appears as HD at m/z = 3 (Fig. 2C), which arises from D-atom attack on glycerol C-H rather than O-D bonds. The signal at m/z = 2 in Fig. 2D reflects the evaporation of both H_2 and D, which have the same mass, where H_2 is created from H-atom attack on glycerol C-H. Although D atoms almost exclusively break C-H bonds over the stronger O-D bonds, we find that e_s^- preferentially breaks O-D bonds, generating D and $C_3H_5(OD)_2O^-$ (*2*, *13*, *19*, *22*). A detailed analysis of the H_2 and HD signals from $C_3H_5(OD)_3$ indicates that e_s^- generates D and H from glycerol O-D and C-H bonds in the ratio of 3:1 (*13*). This ratio of electron-induced O-D to C-D bond breaking for $C_3D_5(OD)_3$ is expected to be even higher because of the lower zero-point energy and weaker reactivity of C-D bonds relative to C-H bonds.

The most striking distinction between our gas-liquid experiments and bulk liquid studies is shown in Fig. 3. The data provide direct evidence for the creation of D atoms near the surface of glycerol and their evaporation into vacuum. We monitored these D atoms at m/z = 2 from the $C_3D_5(OD)_3$ isotopologue, where there is no interference from desorbing H_2. The TOF distribution shown in Fig. 3A includes dissociative ionization components from parent glycerol or glycerol fragments, D_2O, and D_2, in addition to D atoms themselves. These extra components were subtracted from the distribution after fitting each component with a MB distribution at its parent mass with relative intensities consistent with established mass spectral patterns (table S1). The remaining signal in the distribution at early arrival times was fit by a MB distribution at the D-atom mass in Fig. 3B. Analysis of the D and D_2 signal intensities (table S2) indicates that 43 ± 4% of the D atoms desorb before they react to form D_2, implying that D atoms are created close enough to the surface that desorption and reaction occur simultaneously.

The similar time scales for D-atom desorption and reaction may be used to gauge where these atoms are created by Na-atom ionization in glycerol. D-atom reaction times can be estimated from the 1.0×10^7 M^{-1} s^{-1} rate constant for the analogous $D + (CD_3)_2CDOD \rightarrow D_2 + (CD_3)_2\dot{C}OD$ reaction in D_2O at 287 K (*22*). Using this rate constant and taking into account the 14 M density of glycerol, the half-life ($t_{1/2}$)

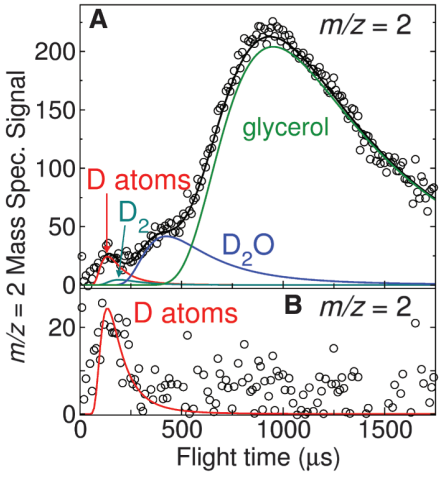

Fig. 3. (**A**) Deconvolution of the m/z = 2 TOF distribution after collisions of Na with $C_3D_5(OD)_3$. The distribution is fit by a sum of D, D_2, D_2O, and glycerol MB distributions at T_{gly}. (**B**) D-atom signal after subtraction.

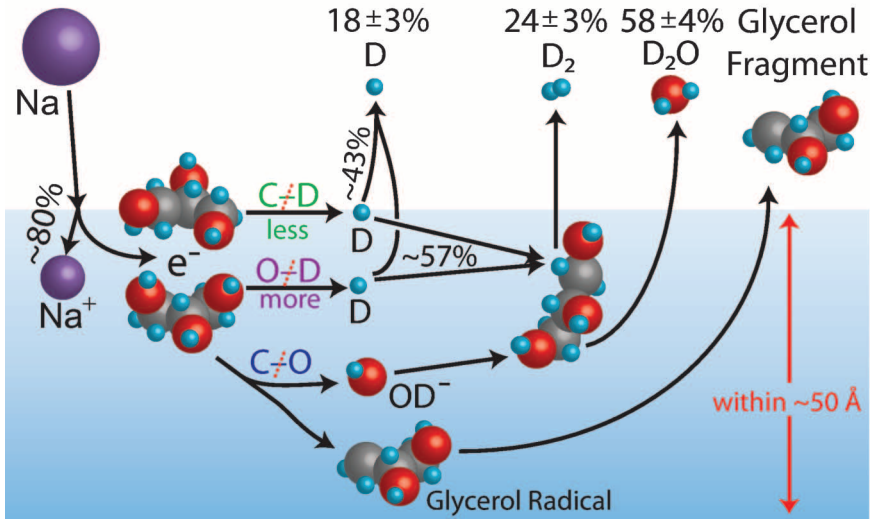

Fig. 4. First steps in the Na atom–initiated electron reactions with deuterated glycerol, $C_3D_5(OD)_3$. Only the OD^- pathway for D_2O production is shown.

for D atoms in pure glycerol is calculated to be 5 ns. D-atom desorption competes nearly equally with D-atom reaction; these atoms desorb on average over a depth of $(Dt_{1/2})^{1/2} \approx 50$ Å, or ~10 glycerol layers, using a diffusion coefficient $D \approx 4 \times 10^{-5}$ cm^2 s^{-1} for D atoms in D_2O (*23*, *24*). This reaction depth may even be shallower if the D atoms diffuse more slowly in pure glycerol because of its viscosity, 2800 cP, at 287 K (*13*). D atoms are therefore created by e_s^- close to, but not necessarily within, the outermost region where Na atoms ionize (*15*).

Figure 4 summarizes the production of D, D_2, D_2O, and glycerol fragments initiated by surface Na-atom ionization, along with possible scenarios for their creation. Each species desorbs only after thermal equilibration. This observation is complementary to the nonthermal ejection of D and O atoms after bombardment of D_2O ice by electrons carrying 5 to 50 eV of energy (*25*), which is substantially greater than the −0.8 eV ionization enthalpy of Na in bulk water (*26*, *27*). Analysis of the TOF signals (table S2) indicates that D, D_2, and D_2O desorb in the flux ratio 1:1.3:3.2. We thus find that nearly half of the D atoms produced by electron-stimulated dissociation of O-D and C-D bonds escape into the vacuum before they abstract a second D atom from the solvent to produce D_2. This high desorption rate implies that near-surface reactions of even this energetic species must compete with its escape into the vacuum—a route that is not available deep within glycerol or other solvents, potentially including aqueous solutions. Because of the proximity of surface molecules to the gas phase, the observed competition between evaporation and reaction should be a universal feature of the interfacial chemistry of neutral energetic species created by interfacial electrons. Alkali-atom collisions provide a promising approach to prepare these electrons and the radicals they create, and to explore their reactions with both solvent and solute molecules at or near the surfaces of liquids.

References and Notes

1. B. C. Garrett *et al.*, *Chem. Rev.* **105**, 355 (2005).
2. G. V. Buxton, C. L. Greenstock, W. P. Helman, A. B. Ross, W. Tsang, *J. Phys. Chem. Ref. Data* **17**, 513 (1988).
3. N. I. Hammer *et al.*, *Science* **306**, 675 (2004).
4. J. R. R. Verlet, A. E. Bragg, A. Kammrath, O. Cheshnovsky, D. M. Neumark, *Science* **307**, 93 (2005).
5. Á. Madarász, P. J. Rossky, L. Turi, *J. Chem. Phys.* **126**, 234707 (2007).
6. D. M. Sagar, C. D. Bain, J. R. R. Verlet, *J. Am. Chem. Soc.* **132**, 6917 (2010).
7. K. R. Siefermann *et al.*, *Nat. Chem.* **2**, 274 (2010).
8. B. Abel, U. Buck, A. L. Sobolewski, W. Domcke, *Phys. Chem. Chem. Phys.* **14**, 22 (2012).
9. A. H. Muenter, J. L. DeZwaan, G. M. Nathanson, *J. Phys. Chem. B* **110**, 4881 (2006).
10. J. Bonin, I. Lampre, P. Pernot, M. Mostafavi, *J. Phys. Chem. A* **112**, 1880 (2008).
11. R. N. Barnett, R. Giniger, O. Cheshnovsky, U. Landman, *J. Phys. Chem. A* **115**, 7378 (2011).
12. M. E. Saecker, G. M. Nathanson, *J. Chem. Phys.* **99**, 7056 (1993).
13. See supporting material on *Science* Online.
14. J. Zhang, D. J. Garton, T. K. Minton, *J. Chem. Phys.* **117**, 6239 (2002).
15. L. Cwiklik, U. Buck, W. Kulig, P. Kubisiak, P. Jungwirth, *J. Chem. Phys.* **128**, 154306 (2008).
16. Y. Ferro, A. Allouche, V. Kempter, *J. Chem. Phys.* **120**, 8683 (2004).
17. R. M. Forck *et al.*, *J. Chem. Phys.* **132**, 221102 (2010).
18. D. H. Paik, I.-R. Lee, D.-S. Yang, J. S. Baskin, A. H. Zewail, *Science* **306**, 672 (2004).
19. J. J. J. Myron, G. R. Freeman, *Can. J. Chem.* **43**, 381 (1965).
20. C. E. Burchill, K. M. Perron, *Can. J. Chem.* **49**, 2382 (1971).
21. J. Park, Z. F. Xu, M. C. Lin, *J. Chem. Phys.* **118**, 9990 (2003).
22. A. M. Lossack, E. Roduner, D. M. Bartels, *J. Phys. Chem. A* **102**, 7462 (1998).
23. E. Roduner, *Radiat. Phys. Chem.* **72**, 201 (2005).
24. V. A. Benderskii, A. G. Krivenko, *Russ. J. Electrochem.* **32**, 663 (1996).
25. T. M. Orlando, G. A. Kimmel, *Surf. Sci.* **390**, 79 (1997).
26. J. O. M. Bockris, A. K. N. Reddy, *Modern Electrochemistry I: Ionics* (Plenum, New York, ed. 2, 1998).
27. H. Shiraishi, G. R. Sunaryo, K. Ishigure, *J. Phys. Chem.* **98**, 5164 (1994).

Acknowledgments: This work was supported by NSF grant CHE-0943639 as part of the Center for Energetic Non-Equilibrium Chemistry at Interfaces. We thank L. Sankaran, G. Schatz, I. Benjamin, and a reviewer for invaluable advice. The data described in this work can be obtained from the corresponding authors upon request.

Supporting Online Material

www.sciencemag.org/cgi/content/full/335/6072/1072/DC1
Materials and Methods
SOM Text
Figs. S1 and S2
Tables S1 and S2
References (*28*–*36*)

31 October 2011; accepted 25 January 2012
10.1126/science.1215956

No Straight Path: Roaming in Both Ground- and Excited-State Photolytic Channels of $NO_3 \rightarrow NO + O_2$

Michael P. Grubb,[1] Michelle L. Warter,[1] Hongyan Xiao,[2] Satoshi Maeda,[2,3] Keiji Morokuma,[2,4] Simon W. North[1]*

Roaming mechanisms have recently been observed in several chemical reactions alongside trajectories that pass through a traditional transition state. Here, we demonstrate that the visible light–induced reaction $NO_3 \rightarrow NO + O_2$ proceeds exclusively by roaming. High-level ab initio calculations predict specific NO Λ doublet propensities (orientations of the unpaired electron with respect to the molecular rotation plane) for this mechanism, which we discern experimentally by ion imaging. The data provide direct evidence for roaming pathways in two different electronic states, corresponding to both previously documented photolysis channels that produce $NO + O_2$. More broadly, the results raise intriguing questions about the overall prevalence of this unusual reaction mechanism.

Traditionally, chemical reaction mechanisms involving multiple bond breaking and formation steps are characterized by a transition state in the form of a well-defined saddle point on the potential energy surface. Recently, however, a second type of mechanism termed "roaming" has come to light, which bypasses this saddle point entirely (*1*–*3*). Instead, a frustrated bond cleavage leaves part of the molecule without sufficient energy to escape, and it orbits the remaining fragment until encountering a reactive site to form the products via intramolecular abstraction. This mechanism has received considerable attention in the past 8 years, having been first identified in formaldehyde dissociation as a minor channel (*4*, *5*) and then later in acetaldehyde as the dominant pathway to $CH_4 + CO$ products (albeit still a minor fraction of the overall quantum yield) (*6*, *7*). Evidence of roaming dynamics has since been observed in a handful of other systems, but in all cases has been observed alongside a traditional tight transition state channel (*2*, *8*).

Recently, we reported that roaming may be the dominant of the two observed pathways that produce molecular products in NO_3 photodissociation (*9*), a reaction of considerable atmospheric importance. Additionally, theoretical calculations implicated roaming on the excited-state potential surface; previous observations of roaming were restricted to the electronic ground state (*10*, *11*). Here, we report direct experimental and theoretical evidence confirming the role of excited-state roaming in NO_3 photodissociation. Thus, roaming is not only the dominant mechanism for forming the molecular products of NO_3 but the exclusive mechanism, with no evidence of a competing traditional transition state.

[1]Department of Chemistry, Texas A&M University, College Station, TX 77842, USA. [2]Fukui Institute for Fundamental Chemistry, Kyoto University, 34-4 Takano Nishihiraki-cho, Sakyo, Kyoto 606-8103, Japan. [3]The Hakubi Center, Kyoto University, Yoshida-Ushinomiya-cho, Sakyo-ku, Kyoto 606-8302, Japan. [4]Cherry L. Emerson Center for Scientific Computation and Department of Chemistry, Emory University, Atlanta, GA 30322, USA.

*To whom correspondence should be addressed. E-mail: swnorth@tamu.edu